Supporting Information for

The Lattice Symmetrization Worked, But With a Plot Twist: Effects of Methylhydrazinium Doping of $MAPbI_3$ on Phase Transitions, Cation Dynamics and Photoluminescence

Mirosław Mączka,*[,a] Maciej Ptak,[a] Katarzyna Fedoruk,[b] Dagmara Stefańska,[a] Anna Gągor,[a] Jan K. Zaręba,[c] and Adam Sieradzki[b]

[a]*Institute of Low Temperature and Structure Research, Polish Academy of Sciences, ul. Okólna 2, 50-422 Wrocław, Poland*

[b]*Department of Experimental Physics, Wrocław University of Science and Technology, Wybrzeże Wyspiańskiego 27, 50-370, Wrocław, Poland*

[c]*Institute of Advanced Materials, Wrocław University of Science and Technology, Wybrzeże Wyspiańskiego 27, 50-370, Wrocław, Poland*

e-mail: m.maczka@intibs.pl

Table S1. The obtained thermal parameters from the DSC measurements of $MA_{1-x}MHy_xPbI_3$.[a]

x	T_1 (T_2) (K)	ΔH (kJmol^{-1})	ΔS (Jmol^{-1}K^{-1})	*N*, by $\Delta S = R\ lnN$
0	330.9^{u}, 328.5^{d}	0.58^{u}, 0.43^{d}, 0.50^{av}	1.79^{u}, 1.35^{d}, 1.57^{av}	1.24^{u}, 1.18^{d}, 1.21^{av}
	(163.8^{u}, 157.1^{d})	2.45^{u}, 2.42^{d}, 2.43^{av}	15.21^{u}, 15.41^{d}, 15.31^{av}	6.23^{u}, 6.38^{d}, 6.31^{av}
0.005	322.8^{u}, 320.1^{d}	0.51^{u}, 0.63^{d}, 0.57^{av}	1.64^{u}, 2.11^{d}, 1.87^{av}	1.22^{u}, 1.29^{d}, 1.25^{av}
	(164.6^{u}, 157.2^{d})	2.47^{u}, 2.52^{d}, 2.49^{av}	15.45^{u}, 16.31^{d}, 15.88^{av}	6.41^{u}, 7.11^{d}, 6.75^{av}
0.021	313.6^{u}, 310.9^{d}	0.59^{u}, 0.41^{d}, 0.50^{av}	2.17^{u}, 1.32^{d}, 1.74^{av}	1.30^{u}, 1.17^{d}, 1.23^{av}
	(164.8^{u}, 158.2^{d})	2.23^{u}, 2.25^{d}, 2.24^{av}	13.80^{u}, 14.35^{d}, 14.07^{av}	5.26^{u}, 5.62^{d}, 5.43^{av}
0.057	292.5^{u}, 289.2^{d}	0.42^{u}, 0.46^{d}, 0.44^{av}	1.48^{u}, 1.79^{d}, 1.63^{av}	1.19^{u}, 1.24^{d}, 1.22^{av}
	(168.6^{u}, 161.3^{d})	2.09^{u}, 2.02^{d}, 2.05^{av}	12.78^{u}, 12.44^{d}, 12.61^{av}	4.65^{u}, 4.46^{d}, 4.56^{av}
0.115	259.3^{u}, 255.6^{d}	0.16^{u}, 0.15^{d}, 0.15^{av}	0.61^{u}, 0.58^{d}, 0.59^{av}	1.08^{u}, 1.07^{d}, 1.07^{av}
	(177.6^{u}, 172.4^{d})	1.34^{u}, 1.34^{d}, 1.34^{av}	7.70^{u}, 7.93^{d}, 7.81^{av}	2.52^{u}, 2.60^{d}, 2.560^{av}
0.207	336.4^{u}, 292.0^{d}	0.84^{u}, 0.49^{d}, 0.67^{av}	2.51^{u}, 1.78^{d}, 2.15^{av}	1.35^{u}, 1.24^{d}, 1.30^{av}
	(286.8^{u}, 207.4^{d})	2.67^{u}, 2.11^{d}, 2.39^{av}	9.19^{u}, 10.83^{d}, 10.01^{av}	3.02^{u}, 3.68^{d}, 3.37^{av}
0.249	337.6^{u}, 292.1^{d}	0.69^{u}, 0.61^{d}, 0.65^{av}	2.05^{u}, 2.29^{d}, 2.17^{av}	1.28^{u}, 1.32^{d}, 1.30^{av}
	(286.7^{u}, 201.0^{d})	3.49^{u}, 2.71^{d}, 3.1^{av}	12.11^{u}, 14.08^{d}, 13.1^{av}	4.29^{u}, 5.44^{d}, 4.83^{av}

[a] Superscripts u, d and av denote heating, cooling and average, respectively.

Table S2. The calculated lifetimes of LE1 emission band of the investigated $MA_{1-x}MHy_xPbI_3$ (x= 0-0.249) samples registered at 80 K and excitation of 450 nm.

$MA_{1-x}MHy_xPbI_3$	τ_1	τ_2
x=0	*3.79*	*28.66*
x=0.005	*10.48*	*45.04*
x=0.021	*8.33*	*37.34*
x=0.057	*9.76*	*46.04*
x=0.115	*15.85*	*55.04*
x=0.207	*36.82*	*150.18*
x=0.249	*36.00*	*202.00*

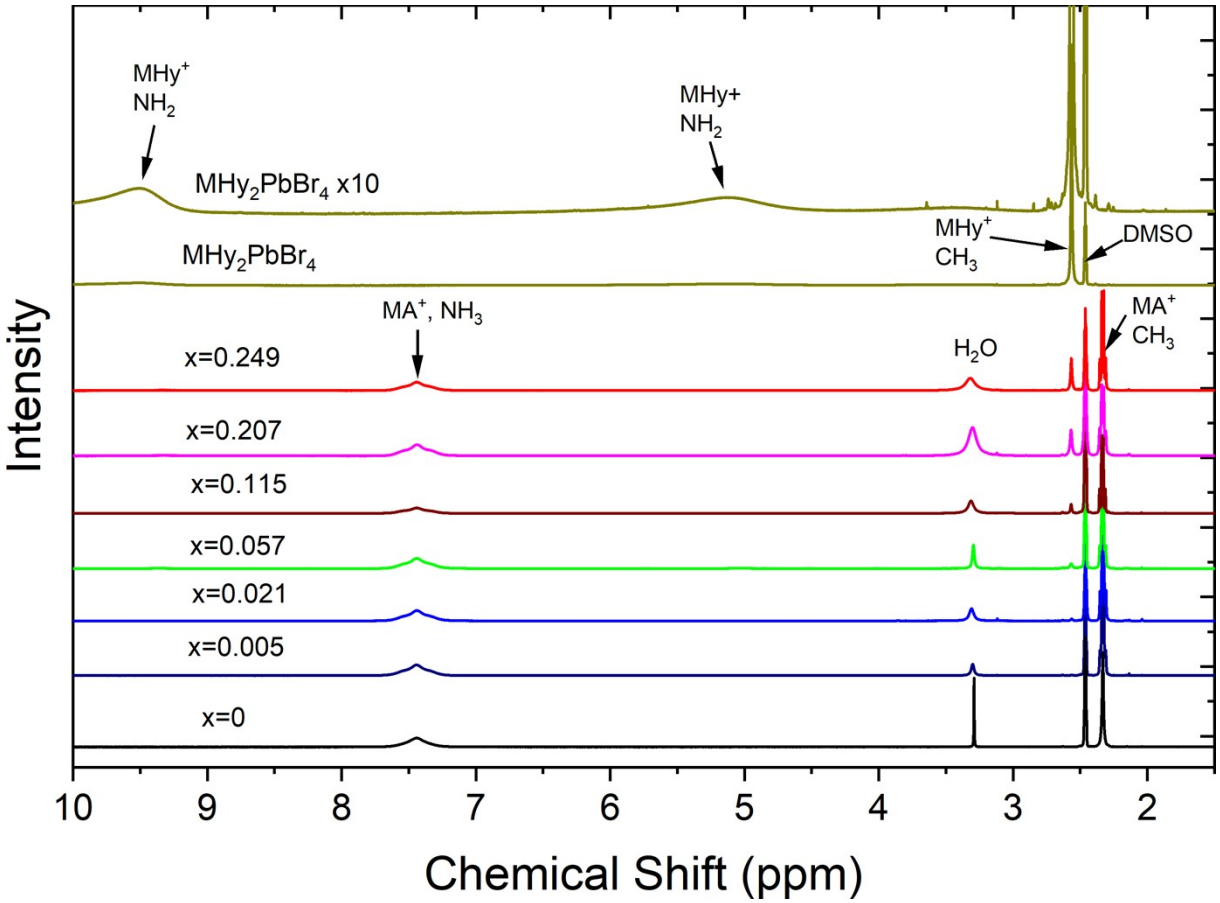

Fig. S1. Room temperature ^{1}H NMR spectra of $MA_{1-x}MHy_xPbI_3$ (x=0-0.249) and MHy_2PbBr_4 in DMSO-d_6.

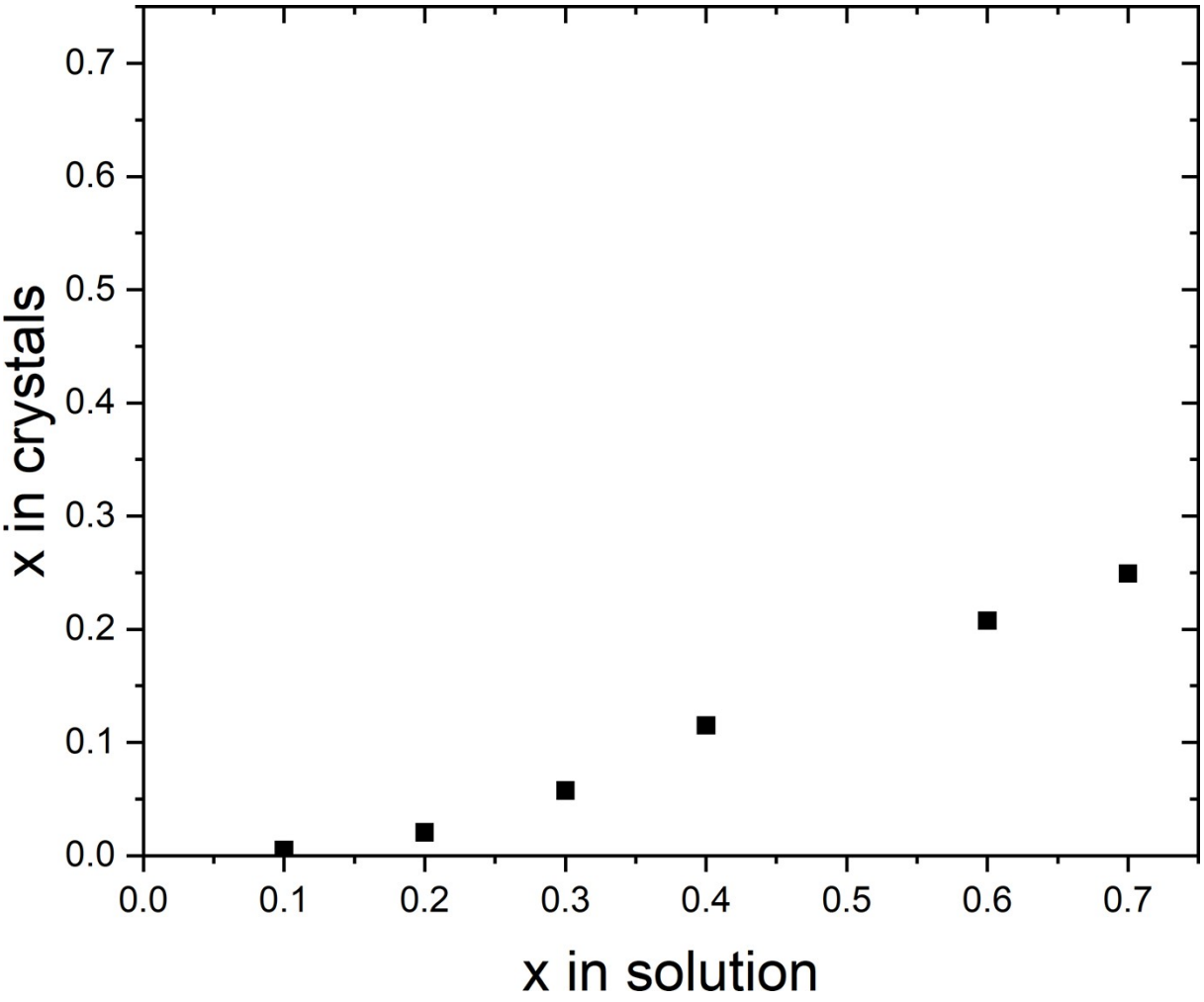

Fig. S2. Dependence of real x in the crystals on x in the solution.

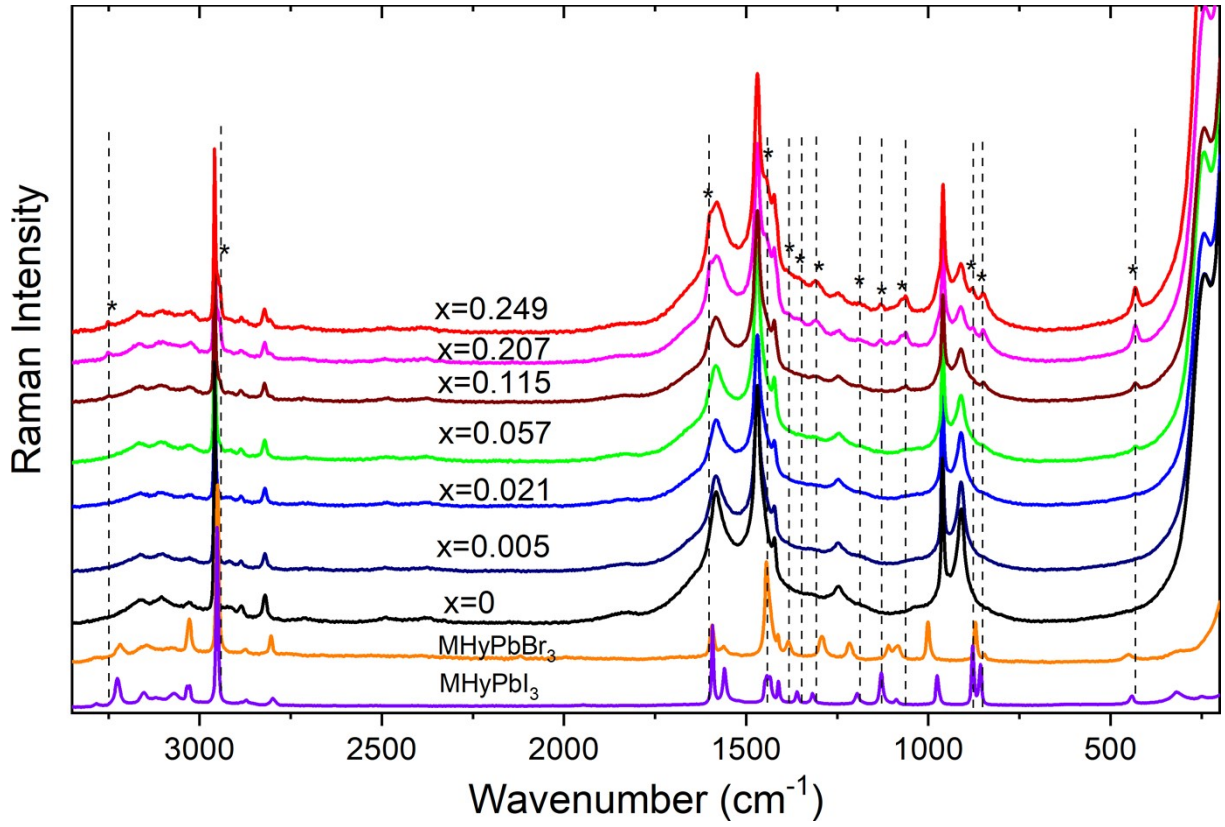

Fig. S3. Room temperature Raman spectra of for $MA_{1-x}MHy_xPbI_3$ (x=0-0.249). For the comparson sake, Raman spectra of 3D $MHyPbBr_3$ and 1D $MHyPbI_3$ are also shown. Asterisks and vertical lines correspond to bands that appears due to presence of MHy^+.

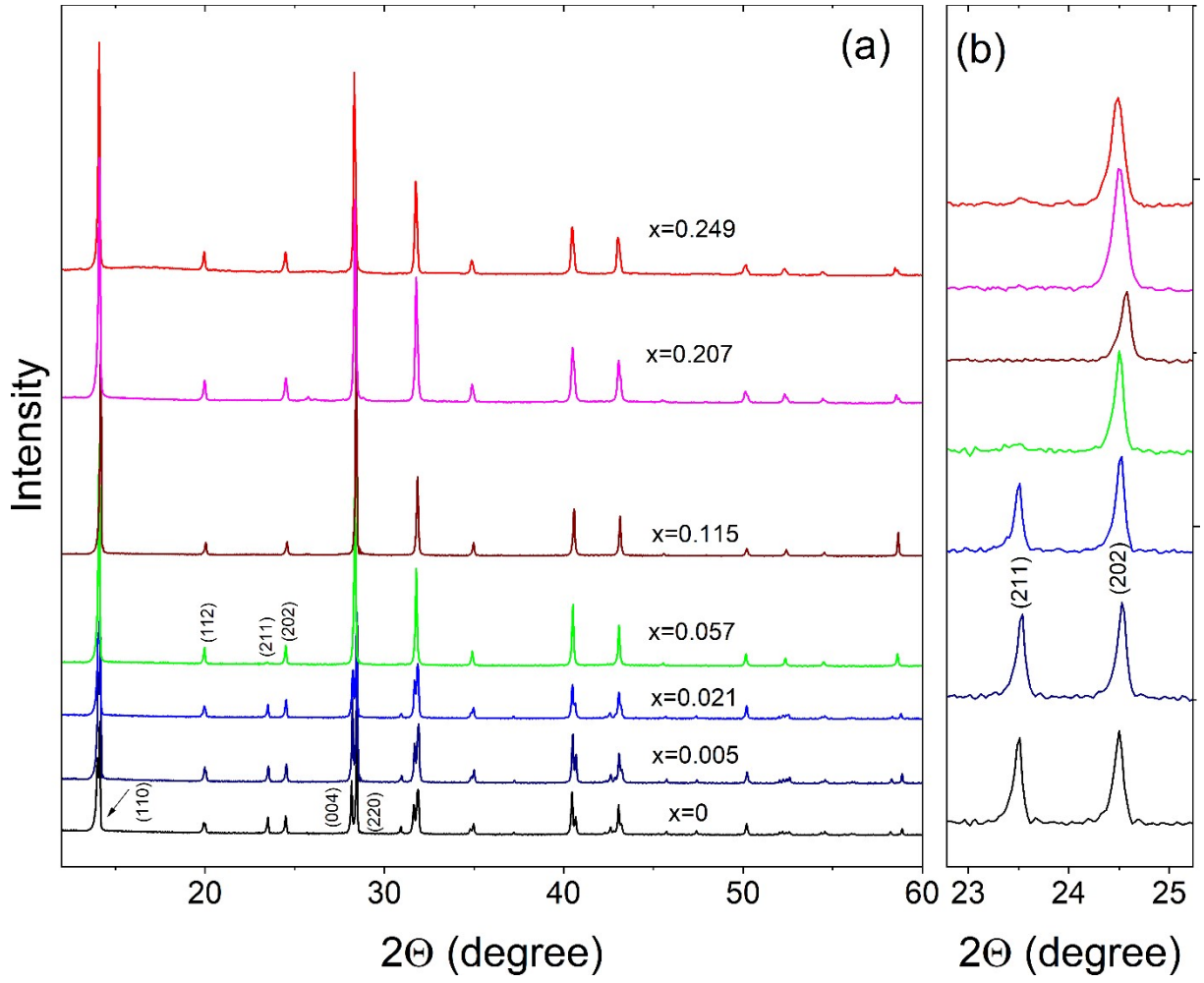

Fig. S4. (a) Powder XRD patterns at room temperature for $MA_{1-x}MHy_xPbI_3$ in the 11-60 degree range; (b) details in the 22.8-25.2 degree, which shows dispapperance of the (211) diffraction peak corresponding to the tetragonal phase for $x \geq 0.057$.

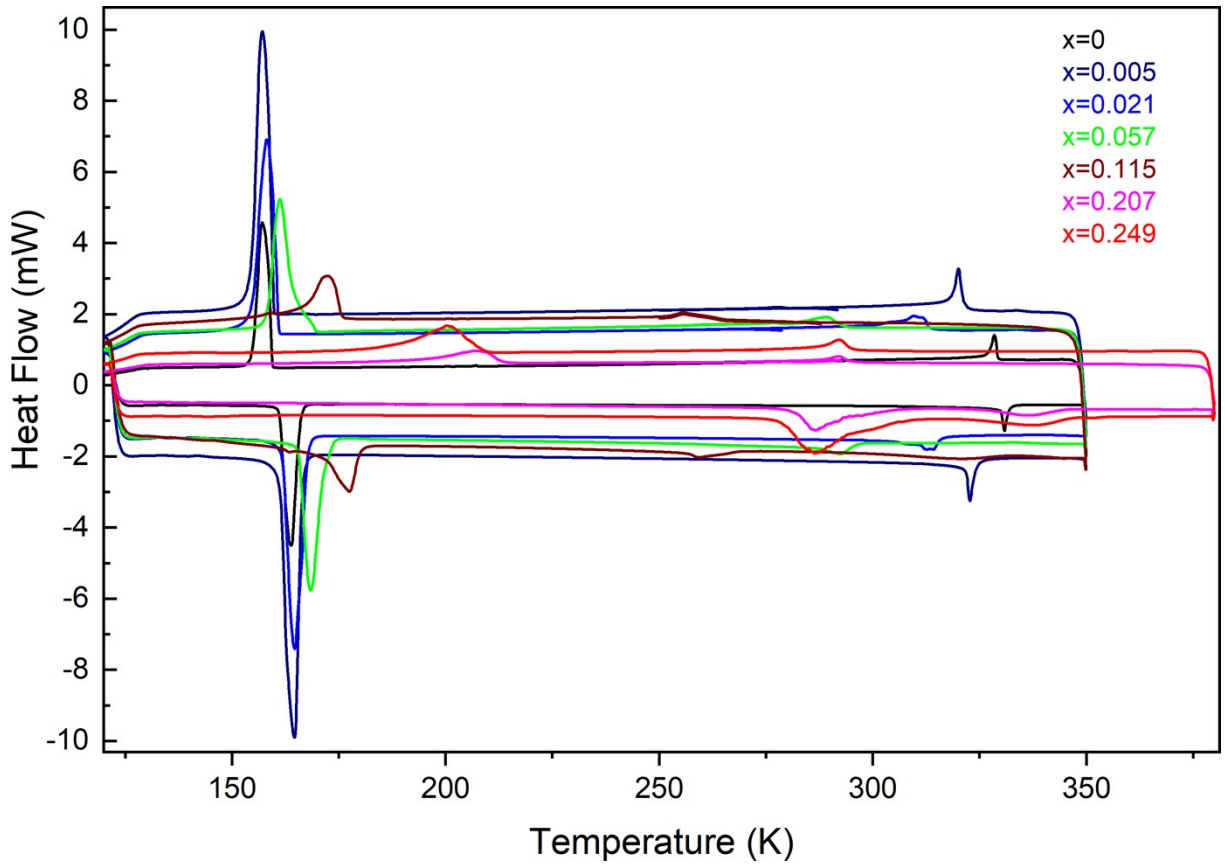

Fig. S5. DSC traces for $MA_{1-x}MHy_xPbI_3$ in heating and cooling mode.

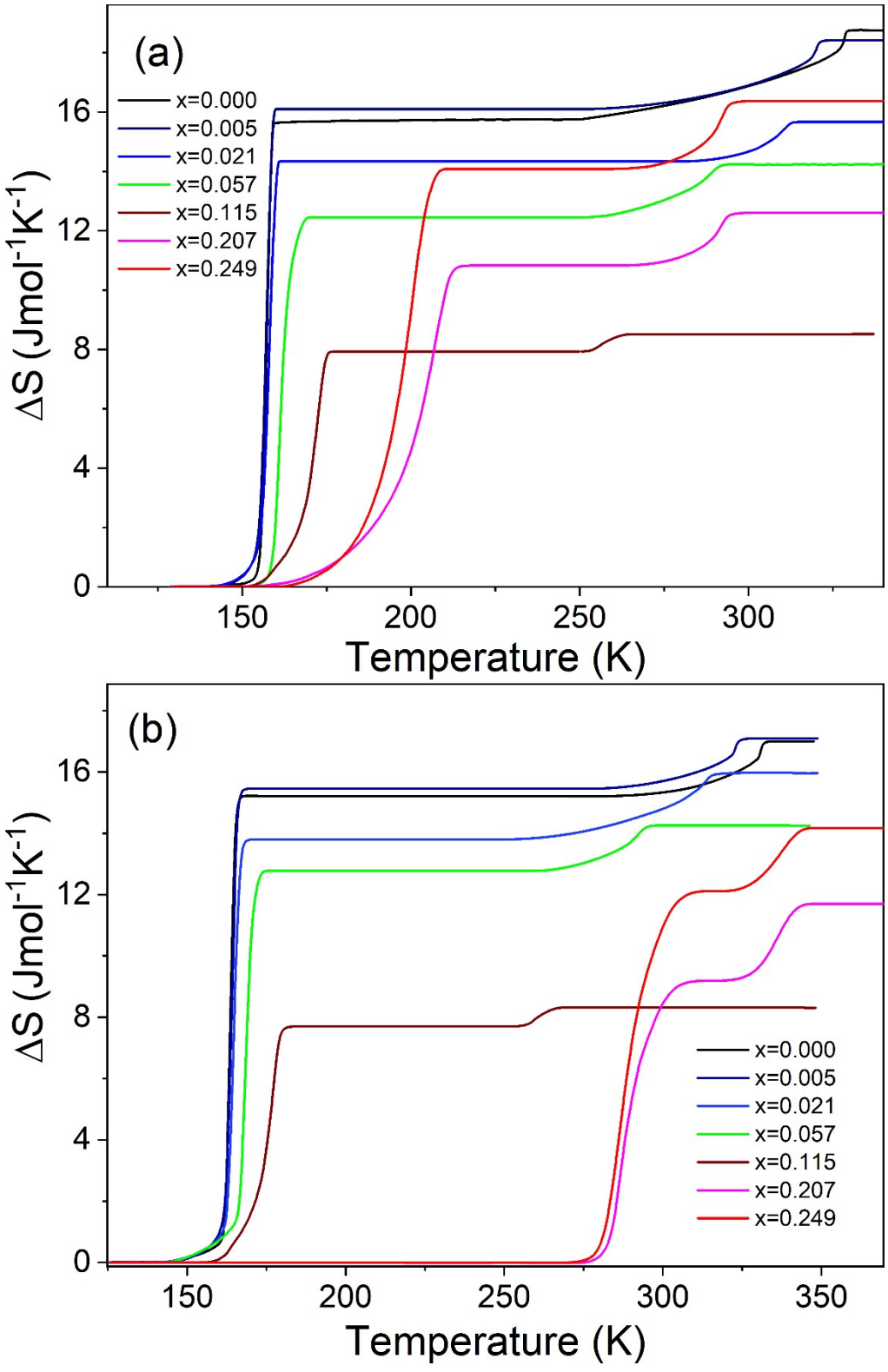

Fig. S6. Temperature dependence of entropy for $MA_{1-x}MHy_xPbI_3$ in (a) cooling and (b) heating mode.

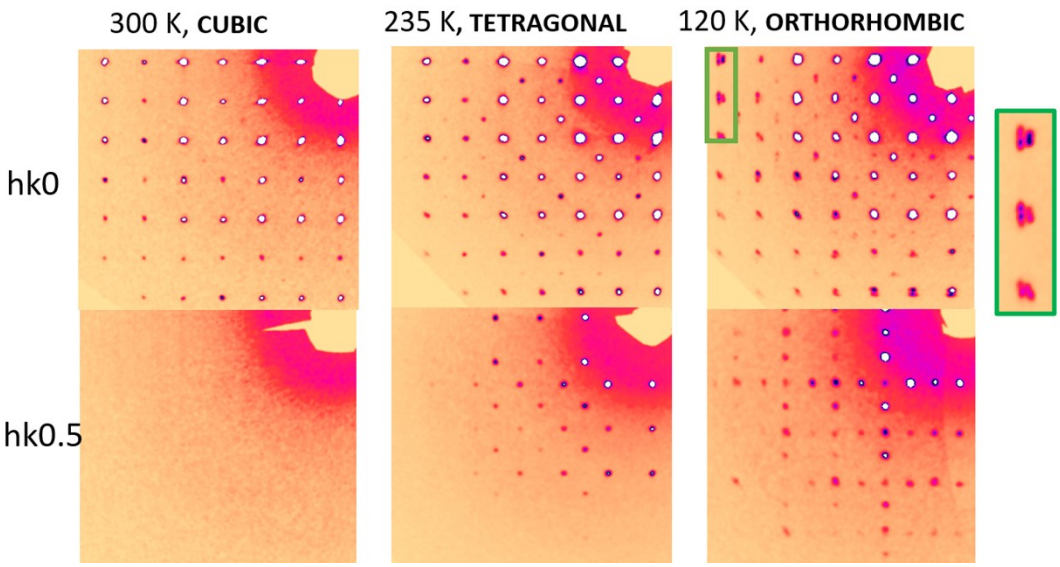

Fig. S7. Reciprocal space reconstructions for x=0.249. The Miller indices refer to the HT cubic prototype phase (a=6.32Å at 300K).

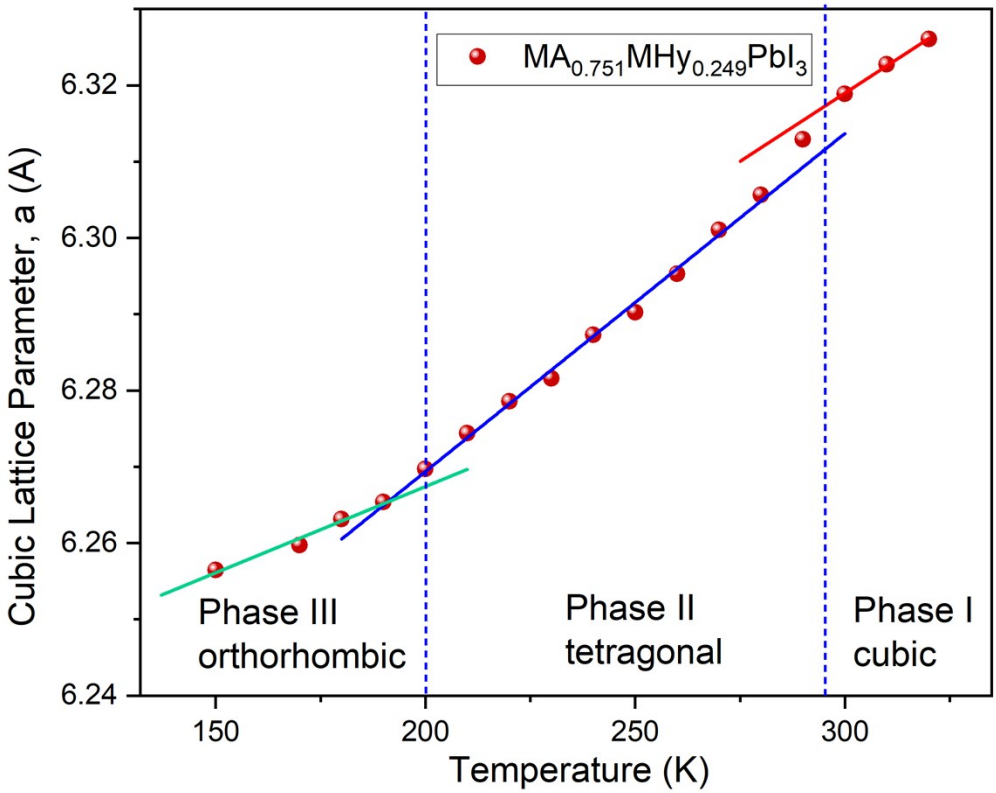

Fig. S8. Thermal evolution of the cubic lattice parameter, calculated over mean positions of Bragg peaks in twinned phases II and III with linear fits in subsequent phases. The lines have been extrapolated to visualize better the changes in lattice contraction. The lattice parameters were calculated from single-crystal x-ray diffraction patterns using 3D profile analysis, integration and fitting (with cubic constrains) performed in CrysAlisPRO (Rigaku Oxford Diffraction).

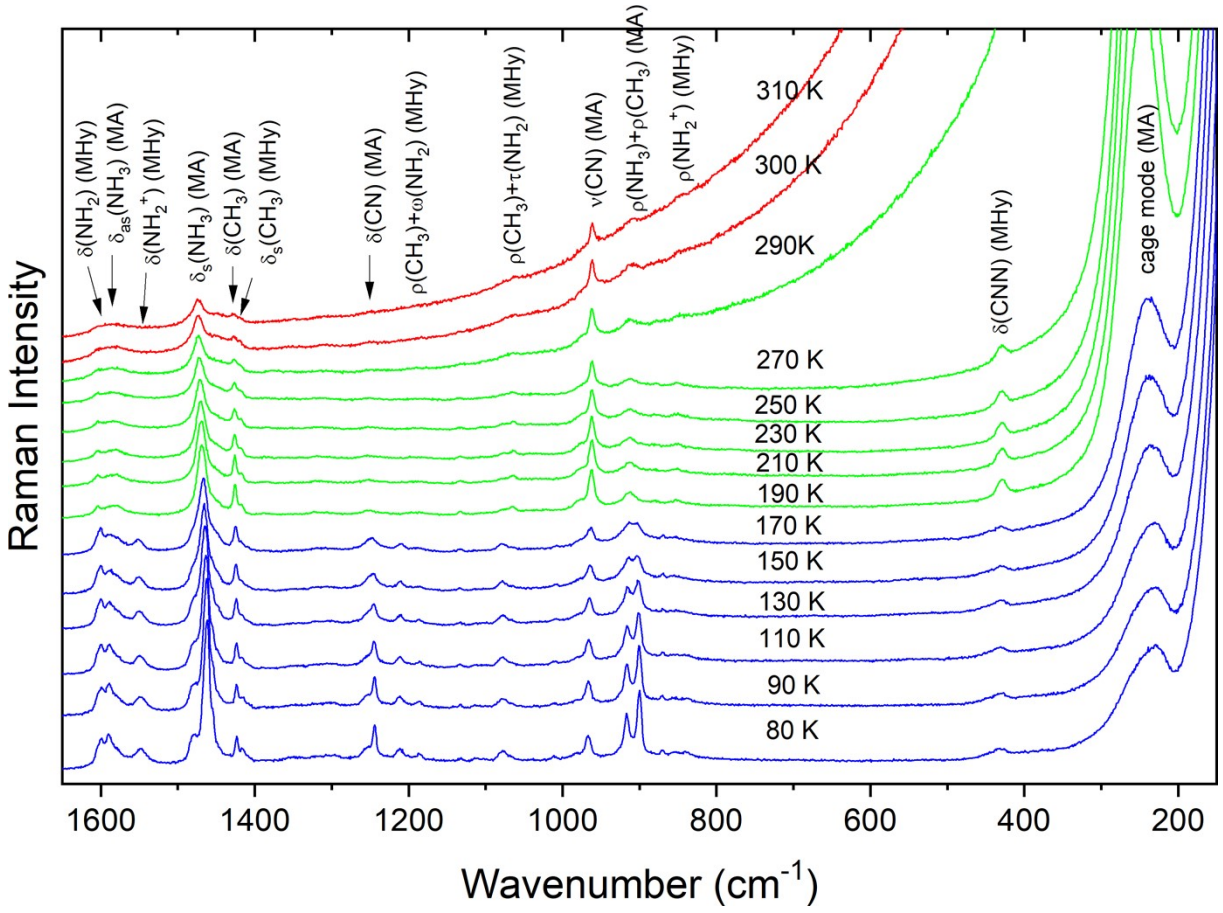

Fig. S9. Raman spectra of the x=0.249 sample in the 1650-150 cm^{-1} range recorded on cooling. Red, green and blue colors correspond to the cubic, tetragonal and orthorhombic phase, respectively.

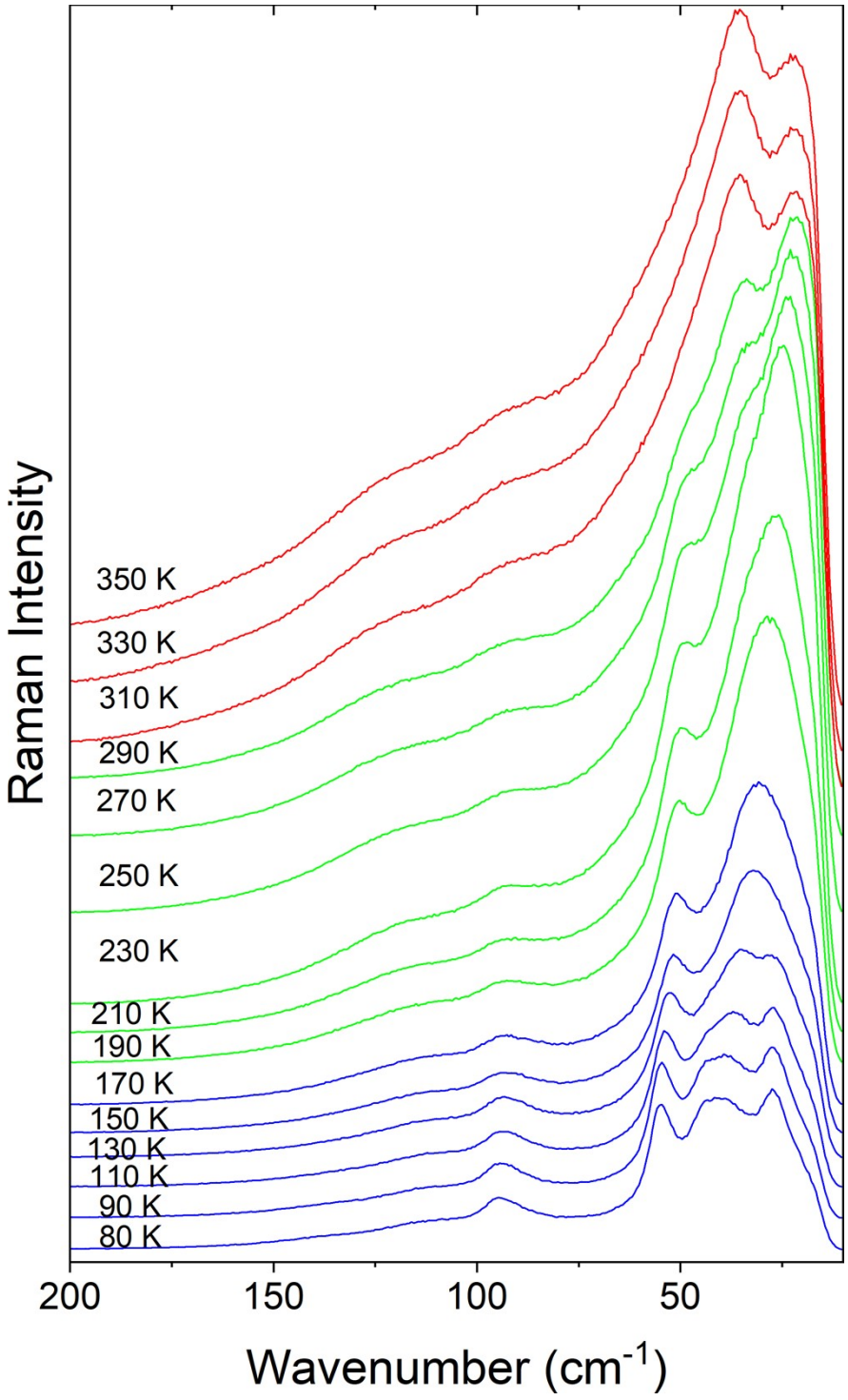

Fig. S10. Raman spectra of the x=0.249 sample in the 200-10 cm^{-1} range recorded on cooling. Red, green and blue colors correspond to the cubic, tetragonal and orthorhombic phase, respectively.

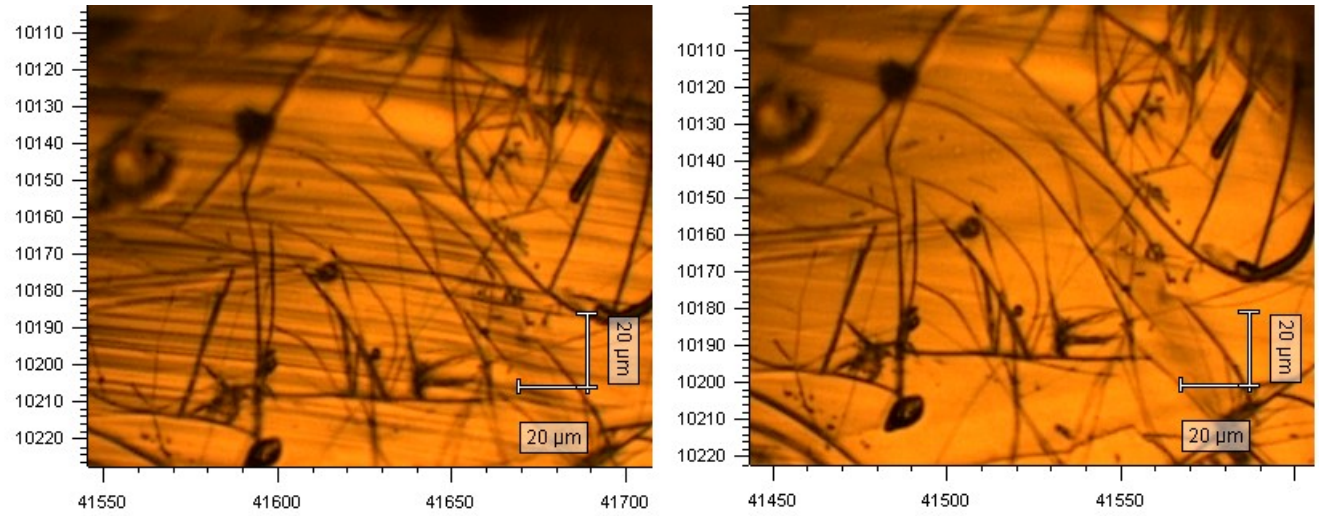

Fig. S11. Photograph of the crystal measured under Raman microscope at 170 K (left panel) and after reheating to 280 K (right panel). Left panel show parallel stripes (domains) that appear at the phase II to phase III phase transition.

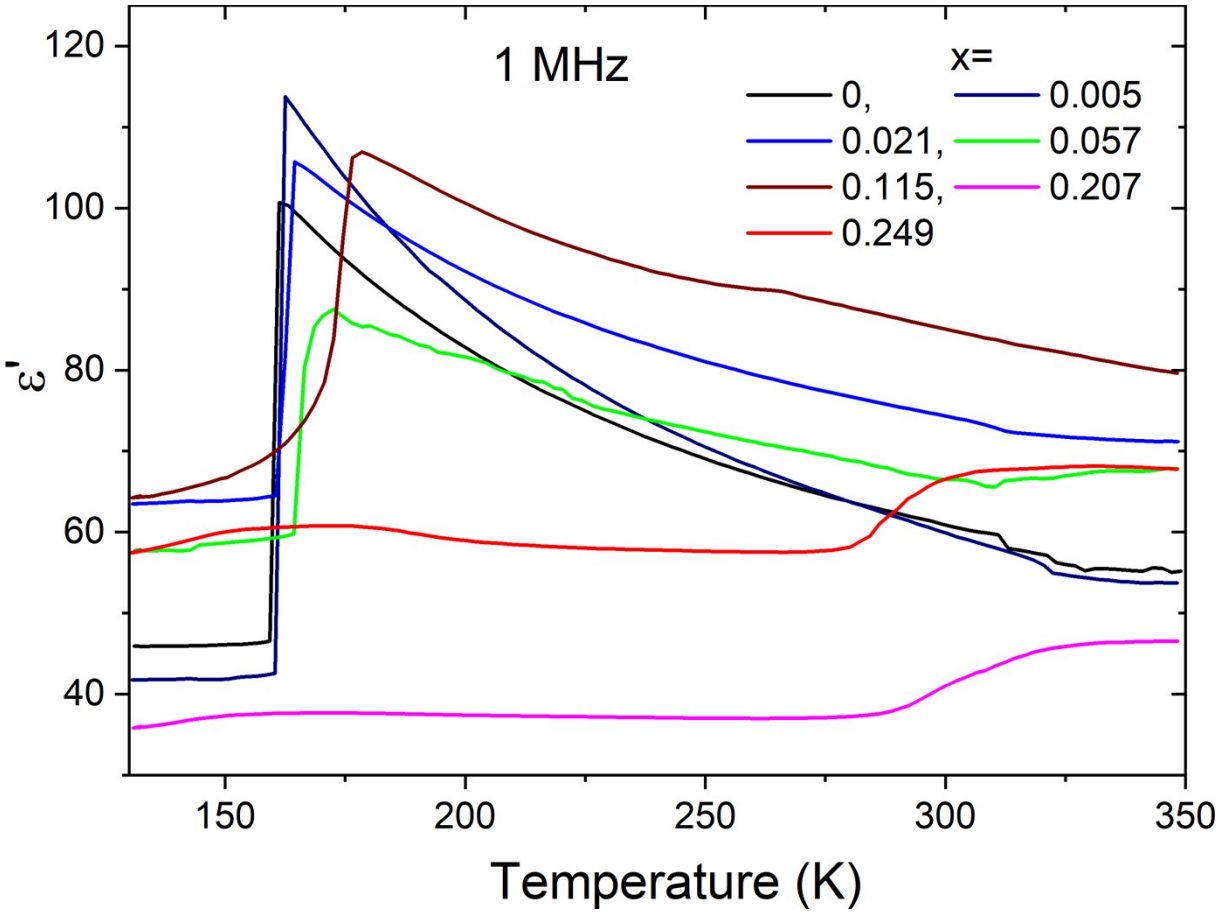

Fig. S12. Comparison of the dielectric permittivity measured at 1 MHz for all studied compositions.

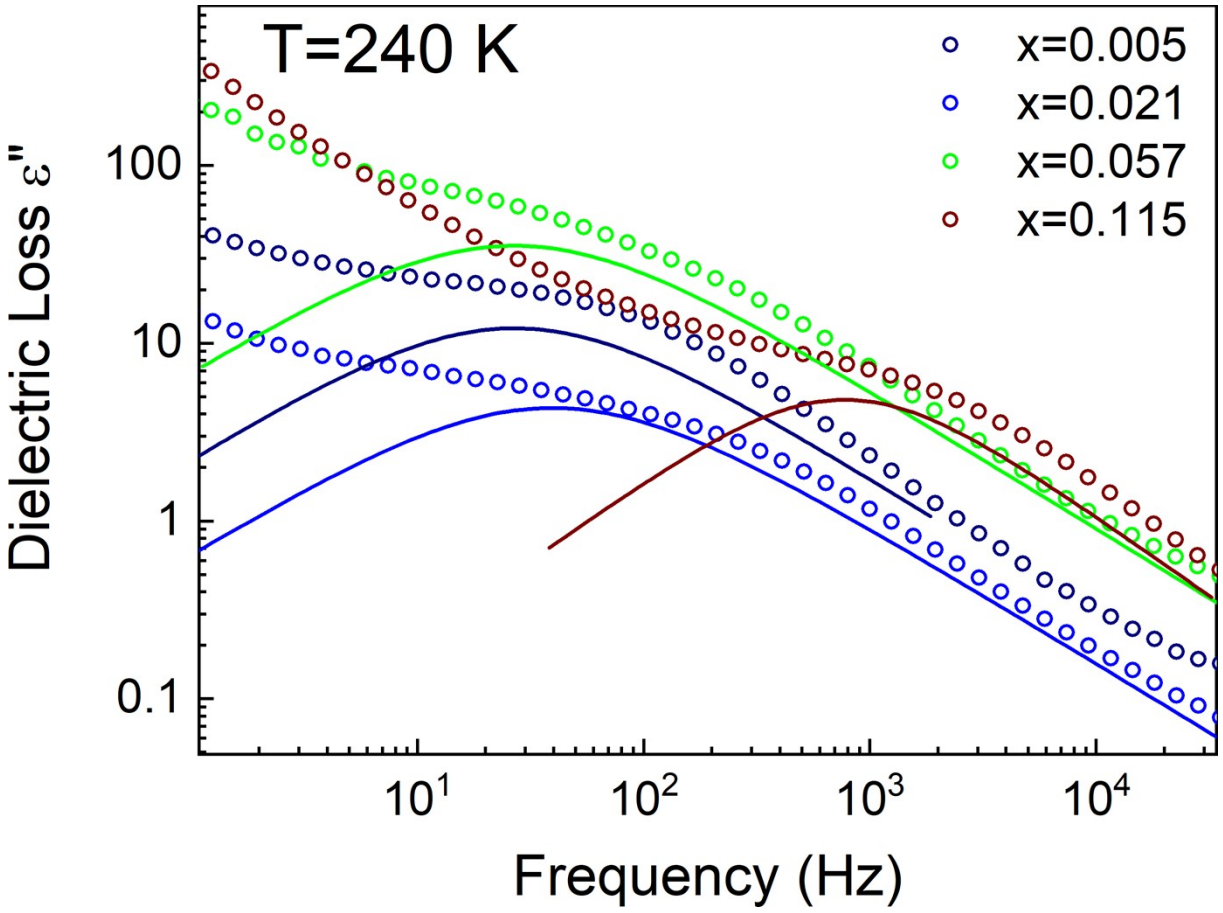

Fig. S13. Dielectric curves as a function of the frequency for selected compounds $MA_{1-x}MHy_xPbI_3$. The solid lines represent the Cole-Cole fit after conductivity subtraction.

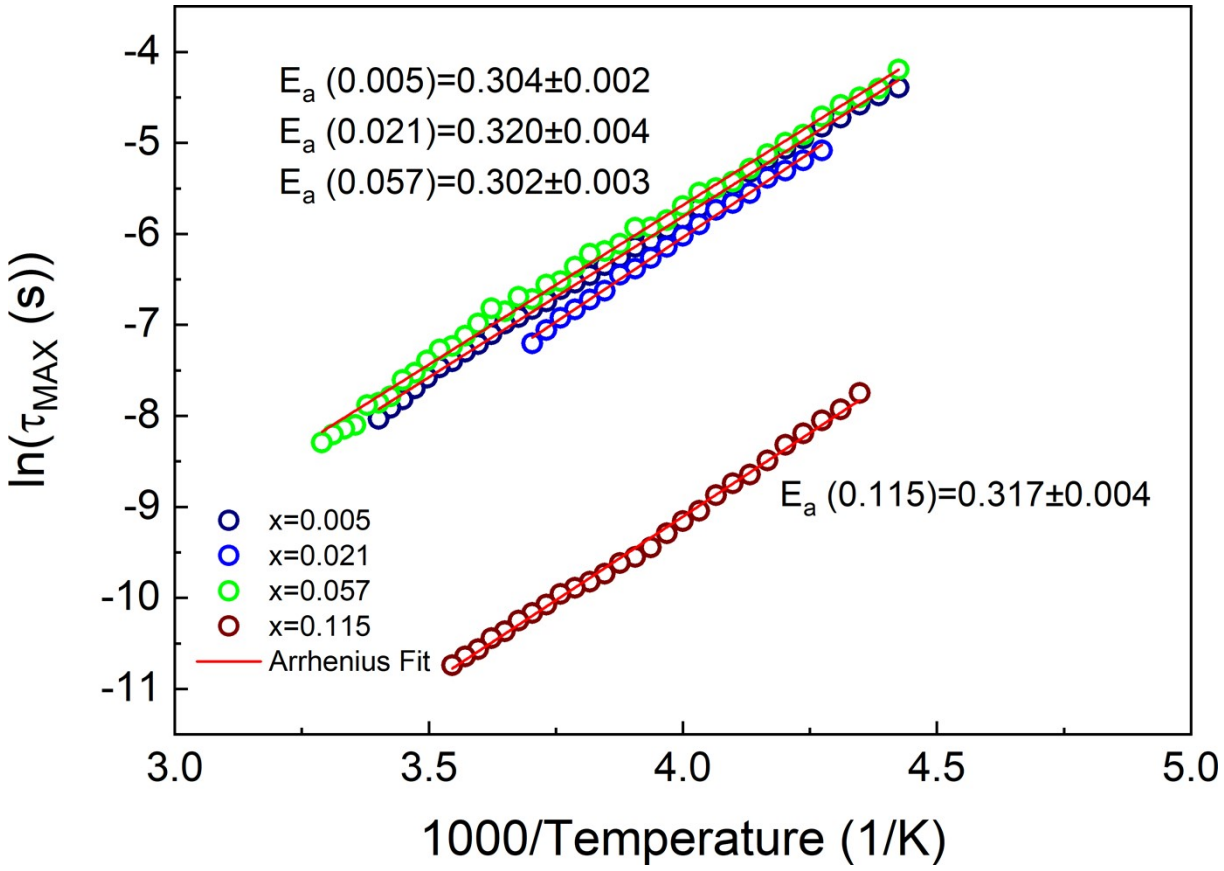

Fig. S14. Inverse temperature dependence of the average relaxation time of the occurring process. Curves indicate fits to the Arrhenius equation.

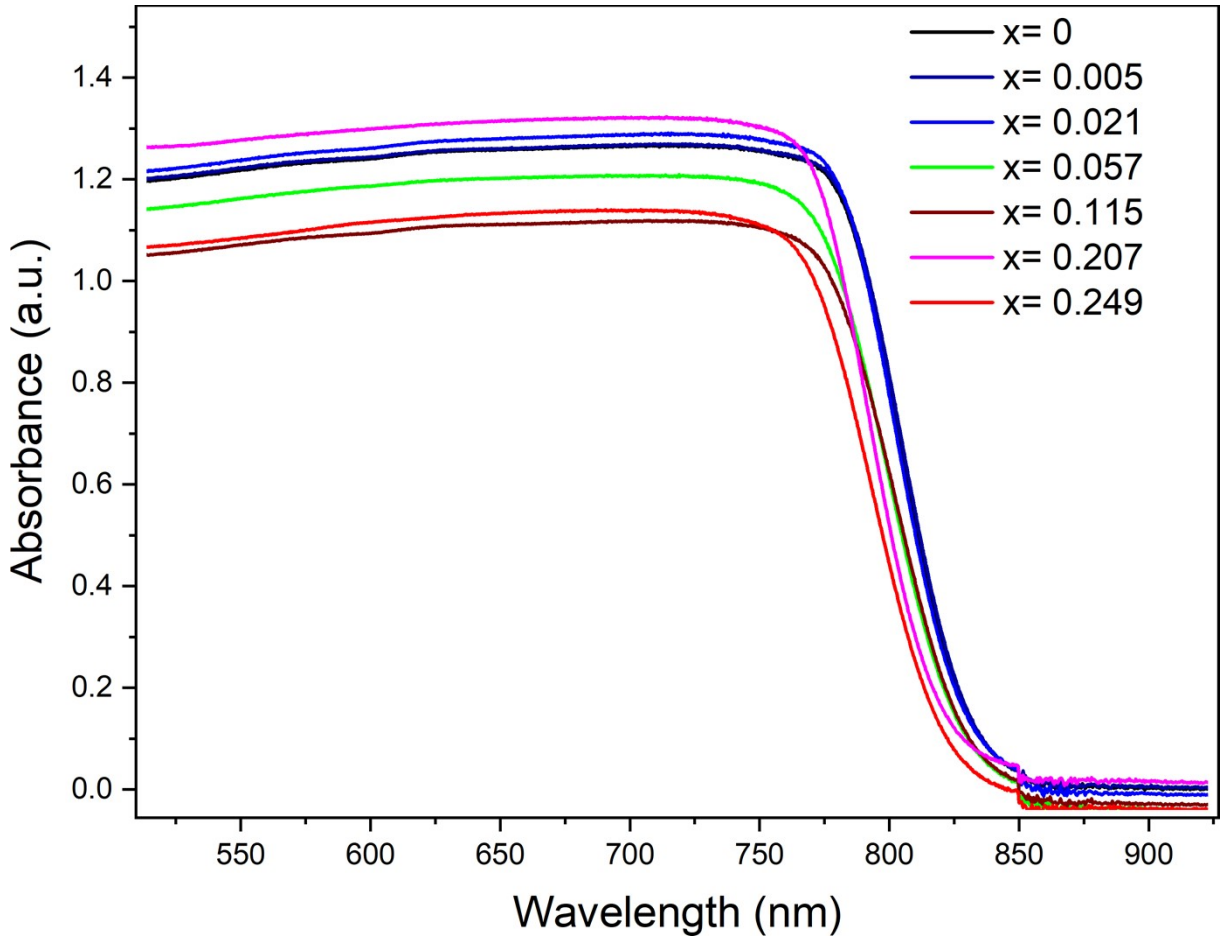

Fig. S15. The diffuse reflectance spectra of $MA_{1-x}MHy_xPbI_3$ samples.

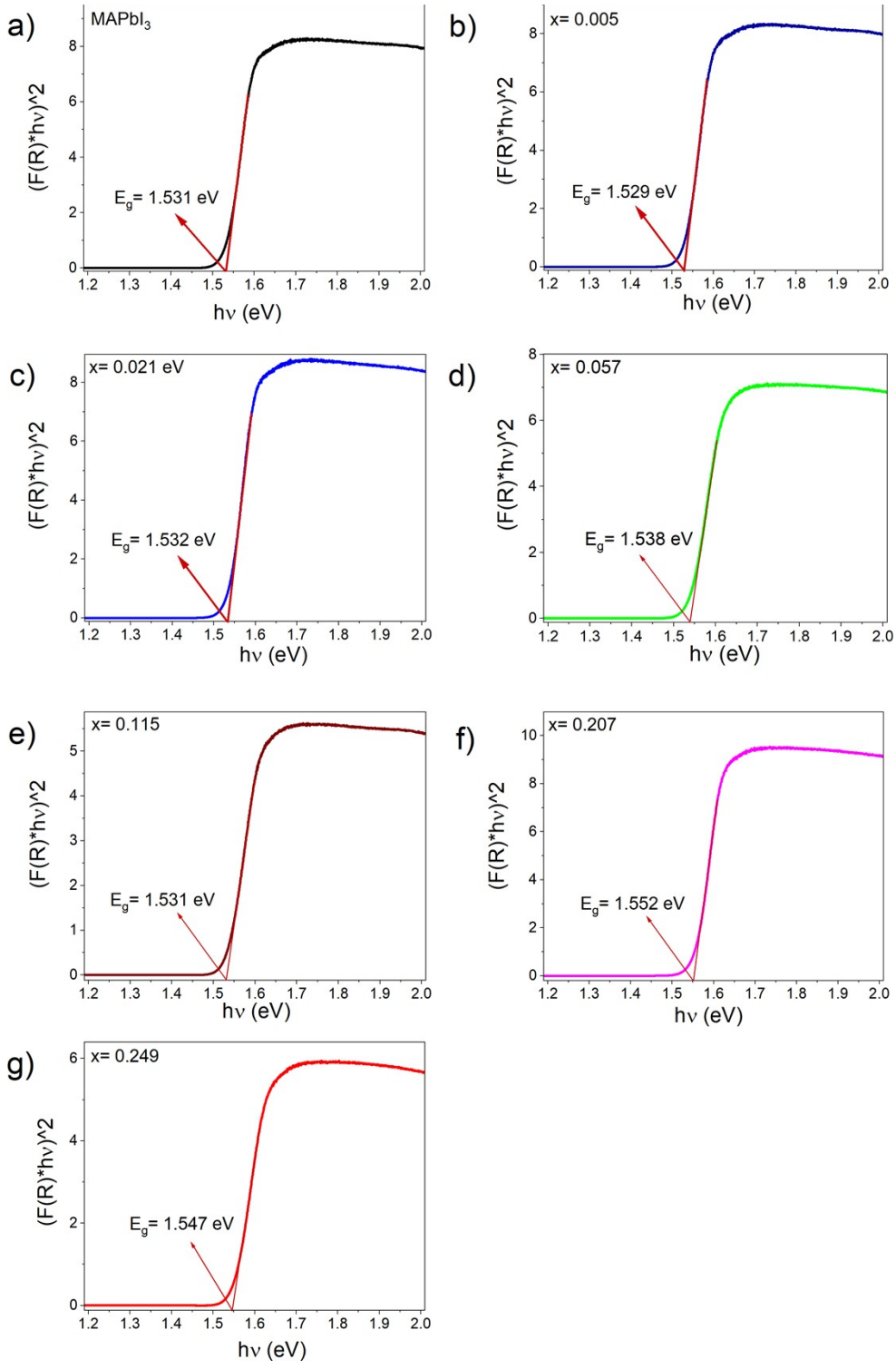

Fig. S16. Kubelka-Munk functions for $MA_{1-x}MHy_xPbI_3$ samples and the energy band gaps (E_g) estimated from the Tauc plots.

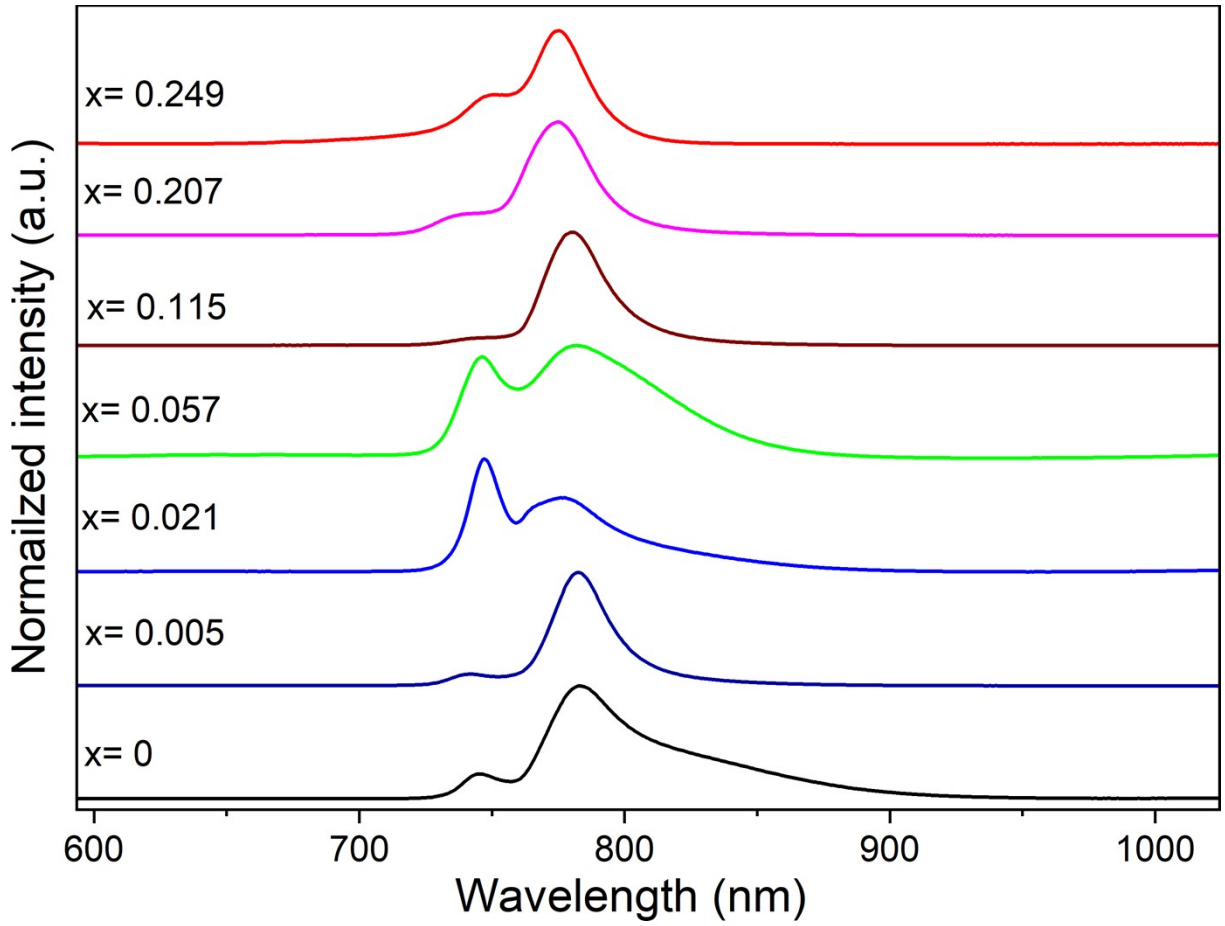

Fig. S17. Normalized PL of $MA_{1-x}MHy_xPbI_3$ samples measured at 80 K.

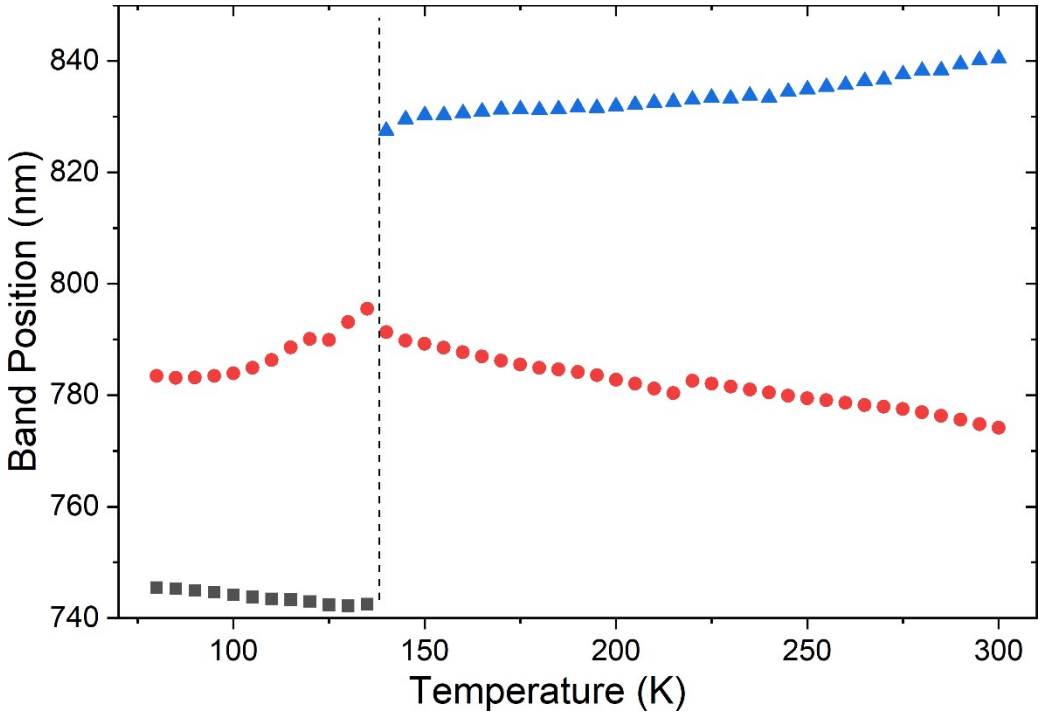

Fig. S18. Temperature dependence of band positions of $MAPbI_3$.

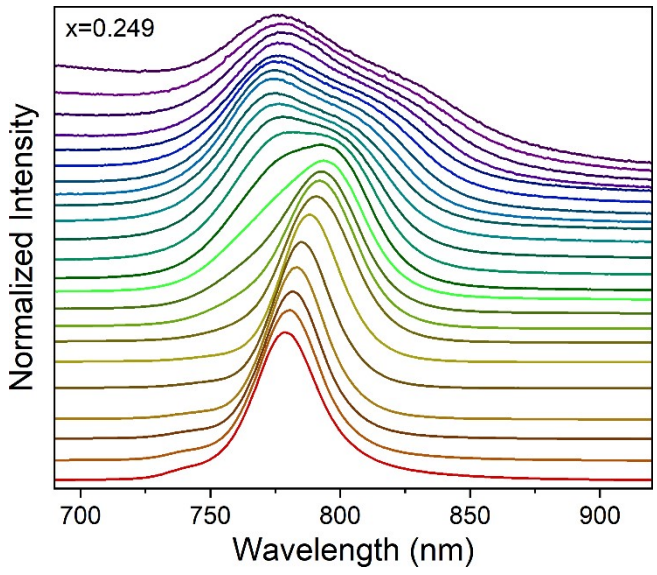

Fig. S19. Temperature-dependent normalized PL spectra of the x=0.249 sample in the cooling run measured every 10 K.

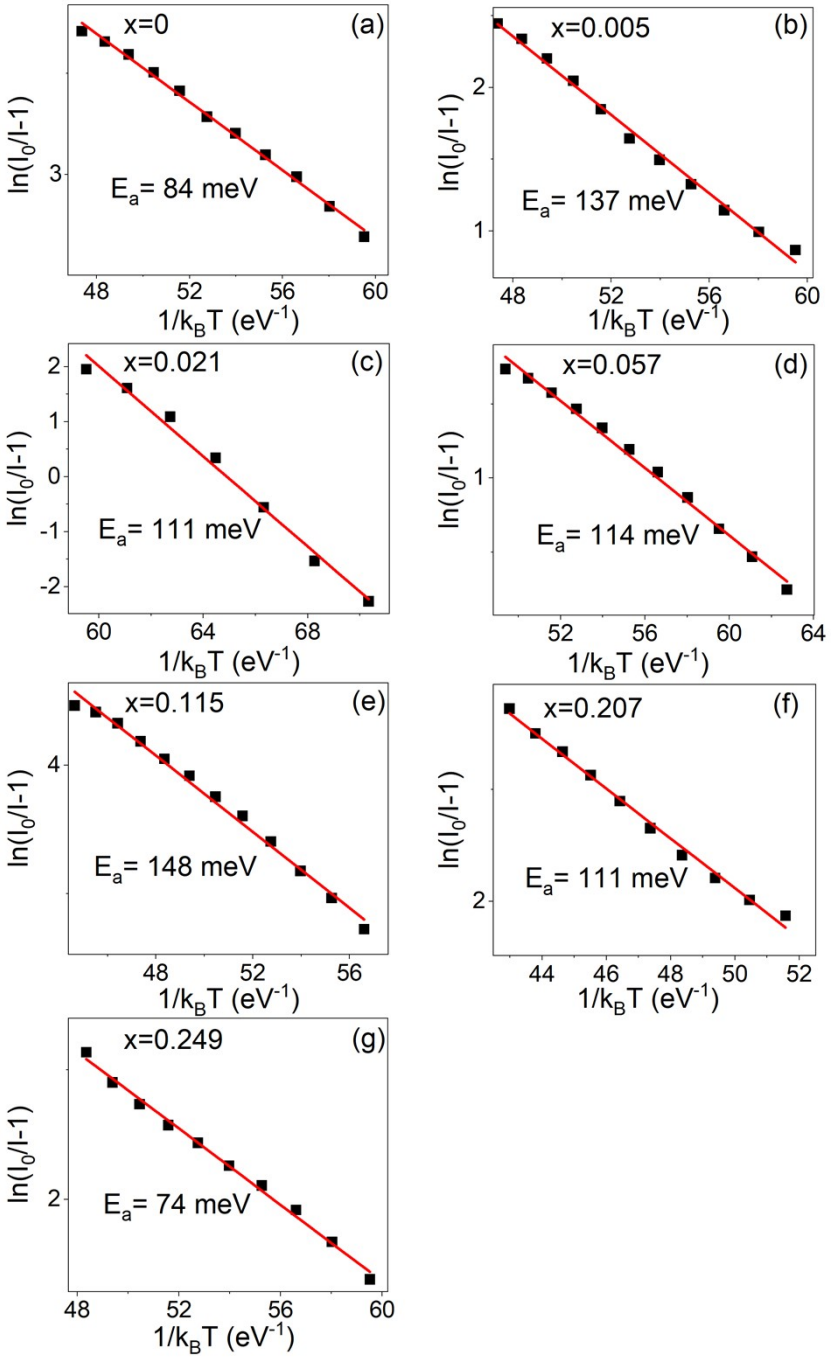

Fig. S20. The exciton binding energy of the $MA_{1-x}MHy_xPbI_3$ (x= 0-0.249) hybrid lead perovskites derived from plots of $\ln(I_0/I-1)$ as a function of $1/k_BT$, where I, I_0 and k_B correspond to LE1 emission intensity at a given temperature, LE1 emission intensity at 80 K and the Boltzmann constant, respectively.

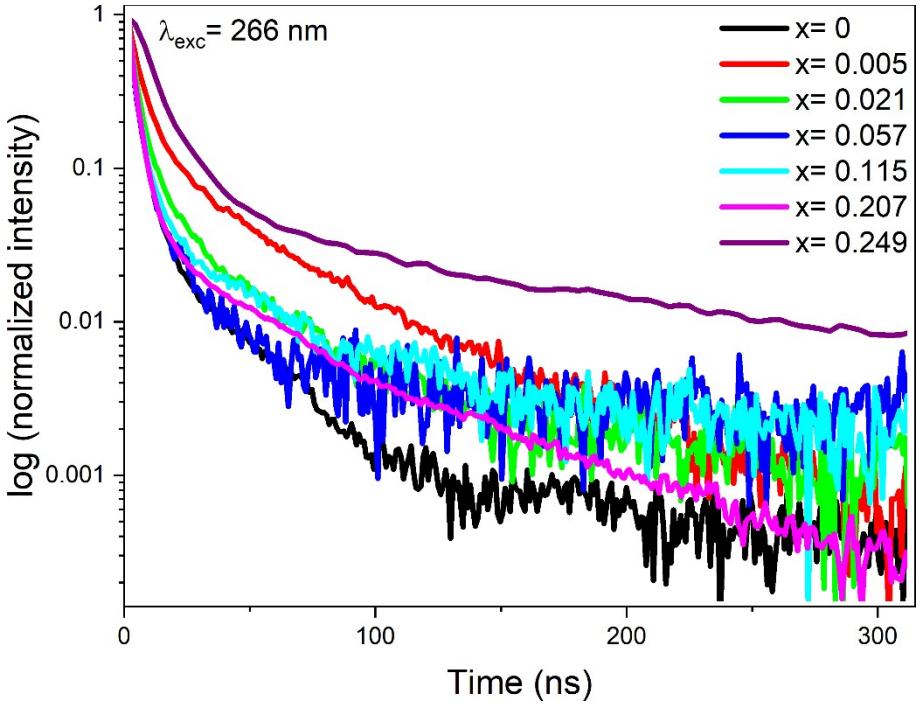

Fig. S21. PL decay curves of LE1 emission of the investigated $MA_{1-x}MHy_xPbI_3$ (x= 0-0.249) samples registered at 80 K and excitation of 450 nm.